

Studies of LBNE Neutrino Flux and Beamline

Amanda Steinhebel

Physics Department, University of Colorado, Boulder, Colorado 80309, USA and

Physics Department, The College of Wooster, Wooster, Ohio 44691, USA

(Dated: August 8, 2013)

The proposed Long-Baseline Neutrino Experiment (LBNE) will produce a neutrino beam whose contents will be measured kilometers away from the facility of production. These measurements will give insight into neutrino oscillation. The beam is produced and focused through a series of independent beamline elements. Misaligning these elements with one another leads to a change in the neutrino flux seen at the far detector. It was found that a 5% flux decrease is observed when the target is misaligned 1 mm, the first focusing horn is misaligned 5mm, or the second focusing horn is misaligned 10 mm. Therefore, the alignment of the initial proton beam on the target is the most crucial aspect of beam alignment for maximum neutrino flux. This final neutrino beam has an analogous direction and energy to the muon beam created through the decay of shared parent pions. This muon beam was also investigated through interactions with a hadron absorber. It was seen for every two muons stopped in the absorber, only one has sufficient energy to escape the absorber and be measured downstream. It was also found that the focusing horns act very much as a lens and can over-focus the beam, resulting in a negatively angled beam when the initial proton beam was offset positively.

I. INTRODUCTION

The Standard Model of particle physics includes three distinct flavors of a nearly massless, electrically neutral particle - the neutrino. The need for such a particle arose due to mysterious findings in the study of radioactive β decay, but today the particle is accepted as fundamental and essential to our understanding of matter. Since they are small, neutrally charged, and only interact through the weak force, neutrinos are extremely difficult to detect. Neutrino beams made of neutrinos from the products of high-energy proton interactions are commonly used to measure properties of neutrinos, such as oscillation. Such a beam is proposed for construction in the United States. Until construction is completed, the geometry can be simulated through the use of a GEANT4 computer simulation [1]. This simulation was used to misalign elements of the beamline and analyze the change in neutrino flux. This information gives insight into tolerances for the elements when construction is underway. A near neutrino detector at the site of the beam's creation is not included in the proposal - instead, the flux of muons through a hadron absorber is tracked. This will yield information about the contents of both the muon and analogous neutrino beam before the neutrino beam is sent to the far detector, and changes in beam composition can be analyzed.

II. NEUTRINO HISTORY AND THEORY

The study of nuclear β decay in the early twentieth-century revealed that electrons are emitted with a full spectrum of energy. This implies that the electron emissions alone do not conserve all energy in the decay. Rather than accept Bohr's idea that energy need not be conserved with every individual event, Pauli proposed a

“desperate remedy” of the neutron - later renamed neutrino. This fermion must be electrically neutral, have spin 1/2, and have a mass on the order of magnitude of the electron [2]. If β decay involved the expulsion of both an electron and neutrino from the nucleus, the energy that seemed to be missing from the electron could be contained by the neutrino thus ensuring energy conservation. Using this as inspiration, Fermi developed a theory of β decay which made neutrinos a necessity. By the mid-twentieth century, the neutrino became an accepted theory within the physics community [2].

A separate but related mystery in physics at the time was the mechanism that supplied the sun's energy. By this time, the accepted theory involved nuclear fusion. Hans Bethe revealed such a series of particle fusions, called the *pp chain*. This chain required the presence of neutrinos [4]. The *pp chain* is still our best model of solar fusion, and explains why neutrinos are observed from the sun. Other celestial bodies and events such as supernovae, solar flares or winds, and other stars produce neutrinos. These, and neutrinos left from the Big Bang, collectively serve to create a cosmic neutrino background [4].

Neutrinos were first measured experimentally by Reines and Cowan in 1956 from inverse beta decay in a fission reactor [3]. In 1968, solar neutrinos were being investigated in the Homestake mine by Ray Davis *et al.* This famous experiment resulted in one-third of the neutrino flux as expected, leading to the solar neutrino problem [4].

By the 1970s, physicists had developed a Standard Model of particle physics to describe the phenomena that had been observed since the 1930s. This model not only includes the neutrino as a fundamental particle, but requires three distinct types or flavors - electron, muon, and tau [5]. The presence of three different types of neutrinos helps explain the solar neutrino problem. The sun only

produces one flavor, therefore resulting in a measurement 1/3 smaller than expected. Bruno Pontecorvo later theorized that neutrinos can change between these flavors while in flight, which is known as neutrino oscillation, since the particle oscillates sinusoidally between flavors [4].

Though the Standard Model predicts massless neutrinos, modern experiments prove that to not be the case. The oscillation results from mass differences between the flavors. For example, Eqn. 1 shows the probability of a muon neutrino oscillating to an electron neutrino:

$$P(\nu_\mu \rightarrow \nu_e) = \sin^2 2\theta \cdot \sin^2 \left(\frac{\pi x}{\lambda_{osc}} \right). \quad (1)$$

Here, θ represents a mixing angle calculated experimentally, x is a distance measured in meters, and λ_{osc} is the oscillation length in meters, given by $\lambda_{osc} = 2.5E_\nu/\Delta m^2$. Therefore, flavor states are not eigenstates of the Hamiltonian and are actually composed of a sort of quantum superposition of all states [3]. The fact that the neutrino only interacts with the weak force also leads to curious behavior, such as the solitary existence of left-handed neutrinos and right-handed anti-neutrinos.

III. DETECTION

Neutrino detectors utilize materials that allow neutrinos to interact with matter and produce a measurable, charged particle. For example, $\nu_e + n \rightarrow p + e$. Since lepton number must be conserved, in the same way that an electron neutrino produces an electron, muon and tau neutrinos produce muons and taus respectively through interaction with matter. All these charged resultant particles can easily be measured and directly related to the initial presence of specific flavors of neutrinos [3].

This detection technology is coupled to man-made neutrino beams. Beams have the benefit of producing high-energy neutrinos which increase the probability of the particle interacting with the detector. Typical neutrino beams collide high-energy protons with a target to produce, through a series of decays of secondary particles, muon neutrinos or anti-neutrinos. The expected flux of these neutrinos can be calculated and compared to measurements made in far detectors. Typical experiments either measure the disappearance or appearance of a certain flavor, with the change resulting from neutrino oscillations.

IV. LONG BASELINE NEUTRINO EXPERIMENT (LBNE)

Neutrino beams are an effective way of studying the oscillation of neutrinos, since the flux can be measured and controlled. Such experiments are currently running in Japan (Tokai to Kamioka), the US (Main Injector Neutrino Oscillation Search), and Europe (CERN Neutrinos

to Gran Sasso). Collaborators in the United States are proposing a more advanced experiment. This experiment, the Long Baseline Neutrino Experiment (LBNE), includes the production of a neutrino beam at Fermi National Accelerator Laboratory (Fermilab) in Batavia, IL and a far detector 1,300 km away in Lead, South Dakota. The beam's intensity of 1 MW makes it more intense than any modern beam. Unlike other detectors, the far detector would contain liquid argon (LAr) rather than water which provides much more information about the particle. Neutrinos are detected in water through Cerenkov radiation, resulting in ring-shaped signals. The distinction between neutrino flavors is dependent upon the shape of these rings and therefore is hard to distinguish when multiple events occur. Liquid argon, on the other hand, detects through ionization rather than Cerenkov radiation. This allows researchers to watch the entire track of the neutrino from its first leptonic interaction, indicating its flavor, to the direct detection of all daughter particles. The proposed detector would contain 35 kTon of liquid argon, providing a great mass for neutrinos to potentially interact with. The development of such an experiment and corresponding set of facilities would take LBNE to the world's forefront of high-energy research and bring many great minds to work in the United States. The project is currently seeking funding with anticipated construction of the beamline beginning in 2015 and the far site facility in 2017. Operation would begin in 2023.

Since the project now is still a proposal, a simulation of the beamline and beam contents is used to investigate the neutrino beam. The G4LBNE beam simulation is made using a GEANT4 simulation package [1]. This software released by CERN utilizes a Monte Carlo random number generator to model particle interactions with matter and is written in C++. LBNE-specific geometry was integrated into the existing GEANT4 simulation, producing a dynamic program that realistically represents the proposed beam. This final program is known as G4LBNE. It is through this simulation that important aspects of the beam, such as the neutrino flux, can be measured and elements can be tweaked to optimize such a measurement before any actual construction begins.

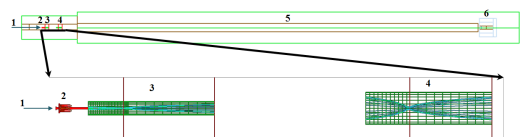


FIG. 1: Visual representation of the LBNE beamline generated by G4LBNE and displayed in HepRApp. 1) Proton/neutrino beam 2) Target 3) Focusing horn 1 4) Focusing horn 2 5) Decay Pipe 6) Hadron absorber

The beam geometry is illustrated in Fig. 1, which was generated through the visualization program HepRApp. The beam, first high-energy protons, begins at 1). It first

encounters a graphite target at 2). This target causes secondary particles such as pions and kaons to be created through interaction with the proton beam. These secondary particles then travel through focusing horns at 3) and 4). Using electric currents to form magnetic fields, these horns focus the desired type of charged particle and deflect the other- similar to a lens to a beam of light. Focusing π^+ results in a beam of neutrinos while focusing π^- produces anti-neutrinos. This focused secondary beam then travels through 5), a decay pipe. Pions naturally decay into muons and neutrinos by $\pi^+ \rightarrow \mu^+ + \nu_\mu$ or $\pi^- \rightarrow \mu^- + \bar{\nu}_\mu$. They travel through a 204 m pipe long enough to allow for this decay, but not long enough to allow muon decay. This beam, now comprised of protons, pions and kaons, muons, and neutrinos, meets a hadron absorber at 6). This absorber is composed of a water-cooled aluminum core surrounded by a layer of steel which itself is surrounded by a layer of concrete. To direct the beam, an aluminum pre-core sits upstream of the core with a hole tapering from a 20 in to 10 in diameter. Figure 2 illustrates this configuration. The radius of the decay pipe does not extend past the steel layer to prevent particles from traveling only through the concrete layer.

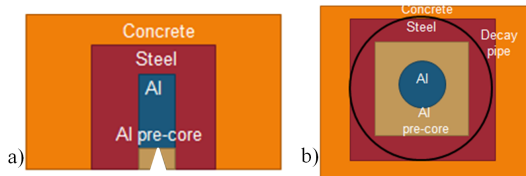


FIG. 2: The configuration of the hadron absorber, including an aluminum pre-core, aluminum core, steel layer, and concrete layer. a) The top view. Notice the taper in the hole in the aluminum pre-core. b) The view from the beamline. The decay pipe radius does not extend past the steel layer, or particles could travel through concrete alone.

The absorber filters out all hadrons and neutrons from the beam. Some muons and all neutrinos are the only beam contents that may exit. These escaping muons hold valuable information regarding the neutrino beam, and are themselves measured after the absorber. They are stopped naturally in the rock following the absorber. The final neutrino beam continues to South Dakota.

V. PROCEDURE

G4LBNE outputs data in the form of trees, which were analyzed with the data analysis software ROOT, released and maintained by the European Organization for Nuclear Research (CERN). The data stored in these trees was accessed through script programs written in C++ and Python which utilize ROOT's analysis power. For the most accurate results, many initial protons on target (POTs) were necessary. Large files with 100,000 or

300,000 POT or a chain of files where the total POT was 100,000 or 300,000 were used to ensure that results are not anomalous.

VI. RESULTS & ANALYSIS - NEUTRINO FLUX

The nominal flux case is shown in Fig. 3. This plot shows the flux of both the total neutrino count and each individual flavor at the far detector. Tau neutrinos and anti-neutrinos are not included because they are not produced in the beam since they are heavier than the original protons. All flux studies involve the total neutrino flux at the far detector.

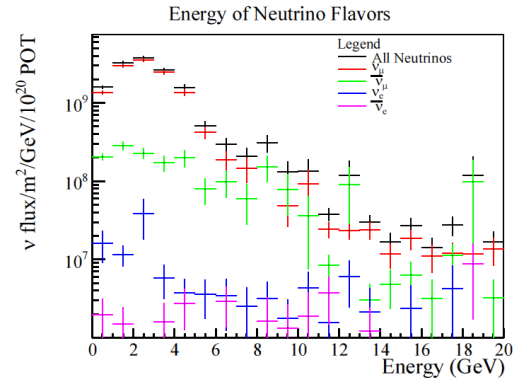


FIG. 3: The flux of the neutrino beam at the far detector is shown, as well as the flux of each flavor that is tracked in the simulation.

The general trend of a flux that peaks at a low energy and decreases asymptotically makes sense. Each decay from the initial high-energy proton causes the daughter particles to decrease in energy, and share that energy unevenly between the daughters. The high-energy tail begins around 10 GeV and remains statistically constant for all high energies.

To analyze the change in flux as a function of beam misalignment, one element was moved in incremented steps and the total flux graph at every offset was recorded. This is demonstrated in Fig. 4. The proton beam itself was moved to an offset of 9 mm in 1 mm increments. This motion occurred near position 1) in Fig. 1, so the offset affects where the beam interacts with the target. The horns are aligned to focus the beam traveling along the z axis, but x offsets move the beam away from the nominal case. The horns cannot focus the beam as well, resulting in the decrease in flux as the offset increases.

All flux readings for offsets greater than 6 mm are nearly identical. With such motion, the beam is no longer hitting the target and instead traveling through air next to the target, explaining the consistent low production of neutrinos. A slight increase in flux can be seen between 6 GeV and 8 GeV for large offsets. This is likely

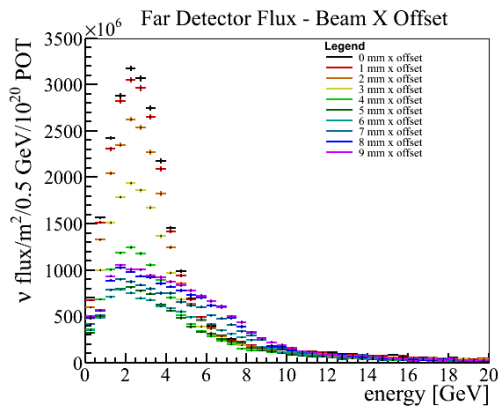


FIG. 4: The flux of the neutrino beam at the far detector is shown as the beam is offset in the x direction.

due to beam interaction with the baffle - a hollow cylindrical graphite tube placed before the target (between the beam production 1) and target 2) in Fig. 1). The baffle serves to keep the beam on target, however beam interaction with the edge of the tube would cause neutrino production in the same way that interaction with the target does. The flux increase is small because the simulated beam production point is inside the length of the baffle. Had the beam been simulated to begin completely upstream of the baffle, the flux would have been expected to increase more between 6 GeV and 8 GeV. This can be seen in detail in Fig. 5.

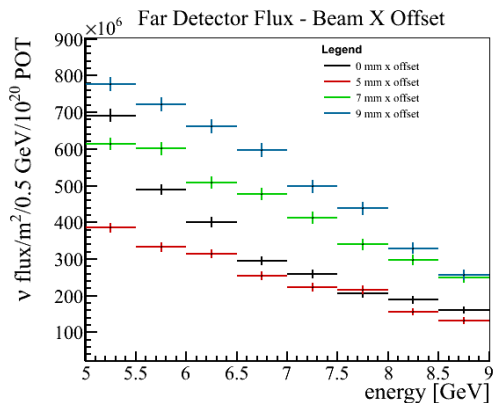


FIG. 5: At large offsets, the beam interacts with a graphite baffle which produces neutrinos much like the target. This increase in flux at the far detector can be seen at offsets such as 7 mm and 9 mm.

Figure 6 illustrates the same data as shown in Fig. 4, but instead displays offset flux values as a ratio between the offset and nominal flux. Again, increased offsets result in decreases in the flux.

Variables to control the x , y , θ , and ϕ positions of the starting beam are included in the input file to the

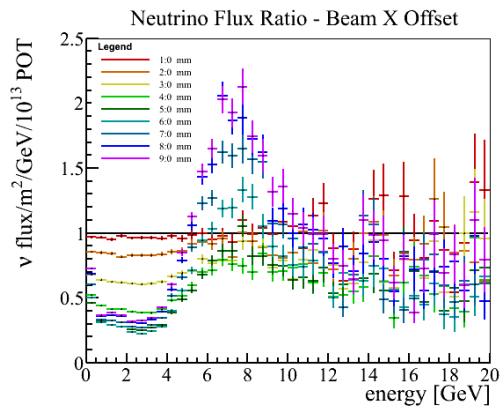


FIG. 6: Flux is shown as a ratio between the flux at the designated offset value and the nominal case.

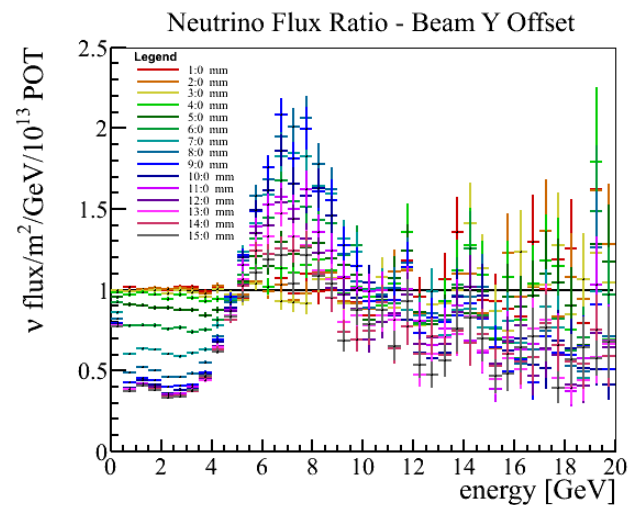


FIG. 7: Flux ratio to the nominal case for incremental offsets of the beam in the y direction, up to 15 mm.

G4LBNE program. Plots such as Fig. 4 and Fig. 6 were made with data obtained from runs with separate input files where the variable is incremented in each.

A similar flux configuration is seen when the beam is offset in y , shown in Fig. 7. Flux resulting from offsets 9 mm or greater do not continue the trend of decreasing flux, similar to the behavior seen in Fig. 6 around 6 mm. This asymmetry in x and y is due to the geometry of the NuMI target, shown in Fig. 8. The shorter x width of 6.5 mm compared to the y length of 15 mm [7] leads to a shorter offset that can realistically be obtained before the beam misses the target entirely.

To analyze the effect of each series of offsets, a new plot using the same data from Fig. 4 was produced. First, the integral of the flux from 0.5-5 GeV, or amount of events per bin, was plotted against the offset value. Error bars were calculated by finding the error of each bin in the

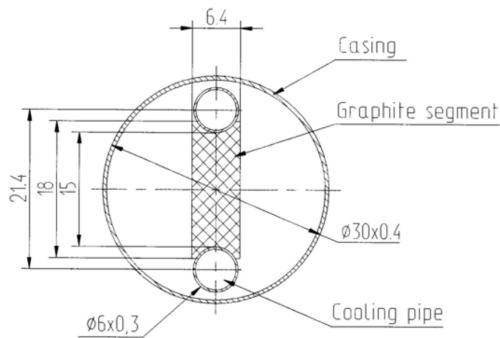


FIG. 8: Visualization of the NuMI target from the NuMI Technical Design Handbook [7]. All measurements are reported in mm, and viewed from the point of view of the beamline. Notice that x and y coordinates are not identical - the target is roughly $6.5 \text{ mm} \times 15 \text{ mm}$, making the y segment longer than the x .

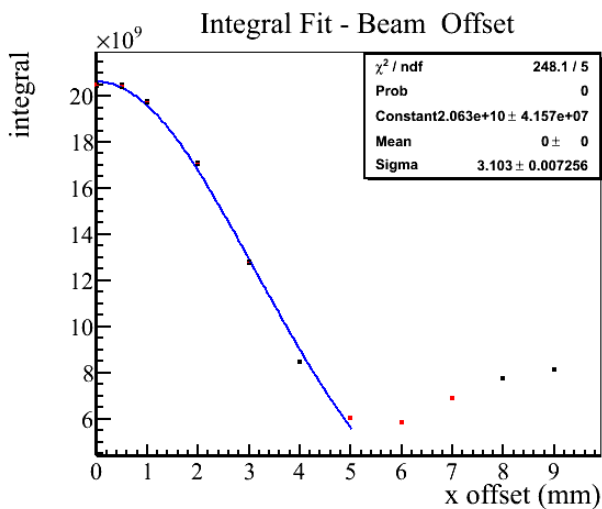


FIG. 9: A Gaussian fit is found to the integral of every offset value. The fit function is found only out to an offset of 5 mm, since any greater offset results in the beam leaving the target.

flux histogram, adding them in quadrature, and taking the square root. This plot was then fit with a Gaussian function, which revealed both χ^2 and σ values for the fit. The corresponding fit plot for Fig. 4 is shown in Fig. 9. The Gaussian function used was set to a fixed mean value of zero to center the curve, and fit to a 5 mm offset. Any greater offset moved the beam off target and eventually interacted with the baffle, so the larger offset data points distract from the true fit of the beam across the target. The σ value of 3.103 ± 0.007256 indicates a close fit to the data, and shows a trend for x offsets.

This study of beam offsets with respect to the rest of the beamline components and their result on the total neutrino flux in the far detector was carried out for

TABLE I: σ and χ^2 values associated with the Gaussian fit of each offset.

Element Offset	Amount of Offset	Gaussian σ	χ^2
Beam x	0-5 mm	3.103 ± 0.007256	248.1
Beam x	0-9 mm	23.9 ± 0.08774	1.925e4
Beam y	0-9 mm	7.237 ± 0.01941	1277
Beam y	0-15 mm	9.404 ± 0.01807	1.523e4
Beam θ (average)	0-5 mrad	3.640 ± 0.04468	337.45
Target x	[-5]-5 mm	2.925 ± 0.01572	18.04
Target y	[-5]-5 mm	31.58 ± 24.63	139.8
Horn 1 x	[-5]-5 mm	28.36 ± 16.83	8.187
Horn 1 y	[-5]-5 mm	18.23 ± 4.627	10.92
Horn 1 z	[-2]-5 mm	22.98 ± 2.259	10.26
Horn 2 x	[-10]-10 mm	63.25 ± 9.812	8.098
Horn 2 x	[-50]-50 mm	107 ± 3.678	25.35
Horn 2 y	[-10]-10 mm	63.24 ± 10.84	13.03
Horn 2 y	[-50]-50 mm	112 ± 4.241	25.58
Horn 2 z	[-20]-20 mm	126.7 ± 11.27	16.77

beam motion in the x and y directions, as well as motion in θ and ϕ . These changes to the beam all occurred upstream of the target. Changes to the angular offsets included an additional variable which set the beam to hit the far detector at the center. To test for cylindrical symmetry, the beam θ was offset from 0 mm to 5 mm for $\phi = 0^\circ, 90^\circ, 180^\circ$, and 270° . The Gaussian σ for each of these separate plots fell within a standard deviation of 0.04316, indicating cylindrical symmetry.

In addition to the beam motion, the target was offset in both x and y directions to compare results to the x and y changes of the beam. Both horn 1 and horn 2 were translated in x , y , and z directions where the beam propagates along the z . For every offset of beamline elements, a different macro file was made, similar to the individual input files necessary for changing the beam. An analogous analysis was performed for each different offset.

Table I shows the σ and χ^2 values associated with the Gaussian fit of the integral of the flux for each offset investigated. Large σ values, or those greater than 10, indicate a poor fit to the Gaussian distribution. This indicates in turn that the change in flux with each offset does not follow a trend and is nearly constant. For example, the large σ value for all fits to horn 2 show that even large changes in the offset of horn 2 only cause small changes in the overall flux at the far detector.

More aspects of this neutrino beam were analyzed than just the flux at the far detector. Scripts in both C++ and Python were written, which inspected characteristics such as the beam position in the xy plane, the beam slope $dxdz$ and $dydz$, the momentum of the initial proton in the xy plane, the source of each individual flavor neutrino which shows which parent is most abundant, the Gaussian fit to the integral of different neutrino flavors,



FIG. 10: The absorber is separated into three distinct sections to analyze. 1) Through the hole in the aluminum pre-core 2) Through the aluminum core, but also through the aluminum pre-core 3) All other parts of the absorber, not limited to that within the area of the decay pipe.

and the parent production vertex in both the xy plane and z direction. The beam position script was used as a check to ensure that offsets moved the beam in its entirety in the designated direction. A shift in the center of the slope graphs could indicate beam motion as well, however analysis of these plots was consistently inconclusive.

VII. RESULTS & ANALYSIS - MUON FLUX

Since there is no near detector in LBNE, an alternate way of identifying the composition of the initial neutrino beam is to analyze the muon flux through the hadron absorber. Muons and neutrinos are both produced in pion decays, as mentioned previously. The muon direction and energy therefore is directly related to the direction and energy of the neutrino, resulting in both muon and neutrino beams that point in the same direction. Charged muons are easier to measure than neutrinos, so these measurements are valuable to understanding the corresponding neutrino beam.

The Conceptual Design Report (CDR) [8] documents measurements for all different sections of the absorber, as shown in Fig. 2. The absorber was divided into three regions, as shown in Fig. 10, from the point of view of the beam (Fig. 2 b)). Region 1 represents a path straight through the absorber along the beamline, passing through the hole of the aluminum pre-core into the aluminum core. Region 2 contains the aluminum pre-core as well as the aluminum core. Region 3 includes every other element of the absorber, not limited to that within the area of the decay pipe. The specifications from the CDR were used in conjunction with the density of each material and its dE/dx vs E plot [9] to calculate the minimum energy necessary for a muon to escape the ab-

sorber. This was done for the center of the absorber (in Region 1) by starting with a 1 MeV muon and stepping backwards through concrete, steel, and finally the aluminum core. The minimum initial energy was found to be 6.178 GeV. In Regions 2 and 3, the minimum initial energy of a muon must be 6.853 GeV and 11.936 GeV, respectively. This minimum energy value can be seen in plots of muons that the absorber stopped and those that escaped. Most muons with energy less than the minimum of 6.2 GeV are stopped in the absorber while most with a greater energy escape. These are shown for total muons in Fig. 11.

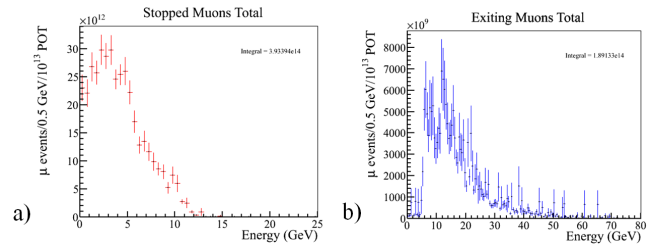


FIG. 11: Muons stopped in the absorber and those with sufficient energy to escape are shown, along with the integral. There are approximately two stopped muons for every exiting muon. a) Stopped muons generally have energies less than 6.2 GeV, the minimum energy necessary to escape. b) Most exiting muons have energies greater than 6.2 GeV.

The printed integral value tells how many muons are present in each plot. It can be seen that for every muon that exits the absorber, two are stopped. The exiting muons are of particular importance. The energy and momentum of these muons is measured in a muon detector downstream of the absorber. This information is then used to correlate the muon and neutrino beams.

These stopped- and exiting-muon measurements can be made for every individual region of the absorber. These plots can also be separated into only μ^+ or μ^- . The typical horn current focuses π^+ and therefore μ^+ , so even low energy μ^+ travel to the absorber. High energy μ^- avoid being deflected by the horns by passing through the neck of the horns where they encounter no magnetic field and still interact with the absorber, but those with low energies are very unlikely to reach that far since they are easily deflected by the horns. There are therefore many more μ^+ than μ^- in runs of this configuration.

Differences between μ^+ and μ^- can also be seen in analyzing the beam shape of both μ^+ and μ^- before and after the absorber. This is shown in Fig. 12. The beam is most intense at the origin, along the beamline. The beam spreads to a radius of about 4 m. Since steel is more dense than aluminum, more muons are stopped in this region of the absorber than the rectangular core. This explains the square-shaped distribution in both μ^+ and μ^- after the absorber.

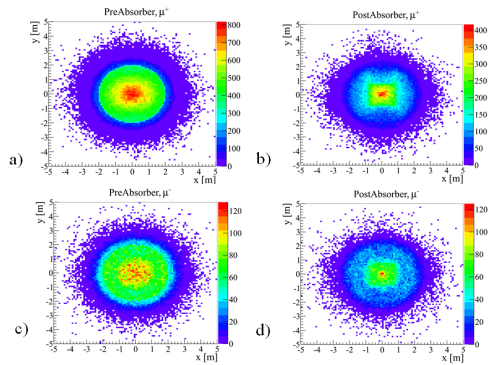


FIG. 12: The μ^+ and μ^- beam positions directly before and after they interact with the absorber.

The muon beam is also helpful to assure that the beam has remained focused on its journey down the decay pipe. Muon beam position can be translated by moving the initial proton beam, similar to earlier neutrino flux studies. The focusing horns act similarly to a lens in focusing the beam, so a beam offset in the positive y direction over-focuses the muon beam and causes it to translate greater in the negative y direction as it travels down the beam-line. This is illustrated in Fig. 13. Here, a nominal case with no beam offset (Fig. 13 a)) is compared to an initial 7 mm beam offset (Fig. 13 b)) resulting in a 13 cm offset of the muon beam immediately upstream of the absorber.

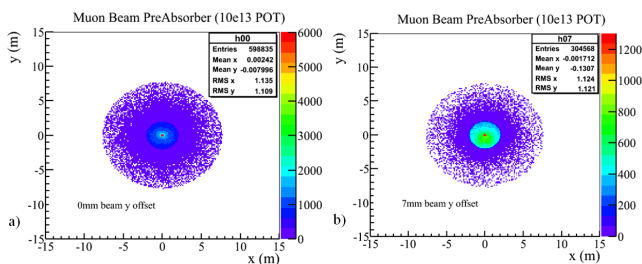


FIG. 13: As the proton beam is offset by $+y$, the muon beam moves in $-y$. The muon beam is shown before it enters the absorber. a) In this nominal case with no beam offset, the muon beam falls at the origin. b) When the proton beam is offset 7 mm, the muon beam moves to -0.1307 m.

VIII. CONCLUSION

A 5% decrease in neutrino flux at the far detector results from a 1 mm offset of the target, 5 mm offset of horn 1, or 10+ mm of horn 2. This shows that the alignment of the beam on the target is the most important aspect of beam alignment for optimum observed flux at the far detector.

The hadron absorber successfully stops 2/3 of all incident muons. The remaining 1/3 that exit can be measured in a detector, and the energy and momentum analyzed to reveal characteristics of the neutrino beam. The muon beam position is also telling of the neutrino beam, and useful knowledge to ensure that the beam has been correctly focused to the far detector. A positive beam offset causes the horns to over-focus the beam, resulting in a negative translation.

Future work involves relating the muon and neutrino beams. This can be done by analyzing only the ancestor particles that created both a muon and neutrino. Their position and momenta off the target can be found. This eventually can lead us to a deeper understanding of the neutrino beam before it is sent to the far detector.

Acknowledgments

I would like to the leadership and guidance of Alysia Marino and Rob Johnson, as well as the LBNE collaboration team, the National Science Foundation, the coordination efforts of Kirsten Paterson, and support of the other participants of this REU program.

- [1] Allison, J. *et al* (GEANT4 Collaboration), "Geant4 developments and applications," *Nuclear Science, IEEE Transactions on*, vol.53, no.1, pp.270,278, Feb.2006. doi: 10.1109/TNS.2006.869826. <http://ieeexplore.ieee.org/stamp/stamp.jsp?tp=&arnumber=1610988&isnumber=33833>
- [2] Franklin, Allan. *Are There Really Neutrinos?: An Evidential History*. Cambridge, MA: Perseus, 2001.
- [3] Schecker, Jay A., and David Kestenbaum. *Celebrating the*

- Neutrino*. Ed. Necita Grant Cooper. Los Alamos, NM: Laboratory, 1997.
- [4] Griffiths, David J. *Introduction to Elementary Particles*. Weinheim [Germany: Wiley-VCH,2008.
- [5] "CERN Accelerating Science." *The Standard Model*. <http://home.web.cern.ch/about/physics/standard-model>
- [6] "About T2K." *The T2K Experiment*. <http://t2k-experiment.org/t2k/>

- [7] “NuMI Technical Design Handbook: Target.” http://www-numi.fnal.gov/numwork/tdh/TDH_V2_4.2.3-Target.pdf
- [8] “Long-Baseline Neutrino Experiment (LBNE): Conceptual Design Report.” <http://lbne2-docdb.fnal.gov:8080/0043/004317/018/volume-2-beam-rev2.pdf>
- [9] “Atomic and Nuclear Properties of Materials for more than 300 materials.” Particle Data Group. <http://pdg.lbl.gov/2012/AtomicNuclearProperties/>